



## Petrographic and geochemical evidence for multiphase formation of carbonates in the Martian orthopyroxenite Allan Hills 84001

Carles E. MOYANO-CAMBERO<sup>1,\*</sup> , Josep M. TRIGO-RODRÍGUEZ<sup>1</sup> , M. Isabel BENITO<sup>2</sup>, Jacinto ALONSO-AZCÁRATE<sup>3</sup>, Martin R. LEE<sup>4</sup>, Narcís MESTRES<sup>5</sup>, Marina MARTÍNEZ-JIMÉNEZ<sup>1</sup>, Francisco J. MARTÍN-TORRES<sup>6,7</sup>, and Jordi FRAXEDAS<sup>8</sup>

<sup>1</sup>Institute of Space Sciences (IEEC-CSIC), Campus UAB, Carrer de Can Magrans, s/n, Cerdanyola del Vallès, 08193 Barcelona, Spain

<sup>2</sup>Departamento de Estratigrafía-IGEO, Facultad de Ciencias Geológicas, Universidad Complutense de Madrid-CSIC, José Antonio Nováis, 12, 28040 Madrid, Spain

<sup>3</sup>Fac. de Ciencias Ambientales y Bioquímica, Universidad de Castilla-La Mancha, Avda. Carlos III s/n, 45071 Toledo, Spain

<sup>4</sup>School of Geographical and Earth Sciences, University of Glasgow, Gregory Building, Lilybank Gardens, Glasgow G12 800, UK

<sup>5</sup>Institut de Ciència de Materials de Barcelona (ICMAB-CSIC), Campus UAB, Bellaterra, 08193 Barcelona, Spain

<sup>6</sup>Instituto Andaluz de Ciencias de la Tierra (CSIC-UGR), Armilla, 18100 Granada, Spain

<sup>7</sup>Division of Space Technology, Department of Computer Science, Electrical and Space Engineering, Luleå University of Technology, Kiruna, Sweden

<sup>8</sup>Catalan Institute of Nanoscience and Nanotechnology (ICN2), CSIC and the Barcelona Institute of Science and Technology, Campus UAB, Bellaterra, 08193 Barcelona, Spain

\*Corresponding author. E-mail: moyano@ice.csic.es

(Received 12 May 2015; revision accepted 30 January 2017)

---

**Abstract**—Martian meteorites can provide valuable information about past environmental conditions on Mars. Allan Hills 84001 formed more than 4 Gyr ago, and owing to its age and long exposure to the Martian environment, and this meteorite has features that may record early processes. These features include a highly fractured texture, gases trapped during one or more impact events or during formation of the rock, and spherical Fe-Mg-Ca carbonates. In this study, we have concentrated on providing new insights into the context of these carbonates using a range of techniques to explore whether they record multiple precipitation and shock events. The petrographic features and compositional properties of these carbonates indicate that at least two pulses of Mg- and Fe-rich solutions saturated the rock. Those two generations of carbonates can be distinguished by a very sharp change in compositions, from being rich in Mg and poor in Fe and Mn, to being poor in Mg and rich in Fe and Mn. Between these two generations of carbonate is evidence for fracturing and local corrosion.

---

### INTRODUCTION

Most Martian meteorites are igneous achondrites. A possible exception is Northwest Africa (NWA) 7034, whose classification is debated, although it is officially described as a basaltic breccia (Agee et al. 2013). Historically, the Martian meteorites have been referred to as “SNC,” although it is now known that some of them do not fit into the three traditional families: shergottites, nakhlites, chassignites (Mittlefehldt 1994; Agee et al. 2013). Martian meteorites have a characteristic

mineralogy, bulk chemistry, and oxygen isotope composition (with NWA 7034 and its pairs being an exception, according to Agee et al. 2013) that distinguish them from other extraterrestrial rocks (McSween 1994; Treiman et al. 2000). The incontrovertible evidence of their Martian origin is the isotopic composition of trapped gas in shock-formed glass, which matches that of the planet’s atmosphere as measured by the Viking lander (Owen et al. 1977; Bogard and Johnson 1983).

In this study, we have studied Allan Hills (ALH) 84001, a 1.93 kg meteorite that was found in Antarctica

in 1984. It was ejected from Mars 15 Myr ago (Nyquist et al. 2001), and fell to Earth ~13,000 yr ago (Jull et al. 1995). Several different crystallization ages have been reported for ALH 84001 (Nyquist et al. 2001; Lapen et al. 2010), thus highlighting the difficulty in dating a meteorite in an open system with a complex postcrystallization history including aqueous alteration and shock metamorphism (Treiman 1998). It is accepted by the scientific community that ALH 84001 is the oldest known Martian meteorite. It formed ~4.1 Gyr ago (calculated using  $^{176}\text{Lu}$ - $^{176}\text{Hf}$  chronometry by Lapen et al. 2010), and during a period of intense bombardment (Frey 2008). Therefore, ALH 84001 is a fragment of Noachian crust, which forms the ancient highlands of Mars (Hamilton et al. 2003). As this meteorite is the only sample we have of the oldest Martian crust, it is a very valuable source of information about the earliest conditions and subsequent evolution of Mars (Bridges et al. 2001).

Once it was recognized as a Martian meteorite, ALH 84001 was classified as an orthopyroxenite (the only one found so far), and therefore is not part of the traditional SNC family (Mittlefehldt 1994). It contains 97 vol% of orthopyroxene ( $\text{Fs}_{27.3}\text{Wo}_{3.3}\text{En}_{69.4}$ ) as grains up to 6 mm in size. Other constituents include 2 vol% of euhedral to subhedral chromite clasts, and 1 vol% of augite, olivine, pyrite, apatite, plagioclase (mostly transformed into maskelynite or glass, by shock), phosphate, and  $\text{SiO}_2$  (Mittlefehldt 1994). The minor minerals are mostly remnants of trapped interstitial melt.

ALH 84001 has a highly fractured texture (Fig. 1), most probably owing to progressive deformation by impacts while it was still on Mars (Treiman 1995). In fact, the meteorite has a complicated shock history, which may have moved it progressively closer to the spallation zone of the impact that ejected it (Melosh 1984). At least two impact events are responsible for its shock features (Treiman 1995); the first event led to brecciation and relocation of the rock closer to the planet's surface, and the second higher intensity event transformed plagioclase into maskelynite or shock-modified plagioclase glass. As a consequence, it has been affected by shock-induced metamorphism. The orthopyroxene and chromite in ALH 84001 are in cumulus phases because of the formation of discrete crystals forming a primary precipitate during slow cooling in a surrounding magma, conforming thus to an orthopyroxene adcumulate (for a description of igneous cumulates, see e.g., Hall 1987). The uniform chemical composition of the pyroxene could indicate that ALH 84001 cooled more slowly than other Martian meteorites during magmatic or metamorphic recrystallization (Mittlefehldt 1994), probably at a depth of ~40 km (Kring and Gleason 1997).

One of the most interesting features of ALH 84001 is the presence of Mg-Fe-Ca carbonates along fractures and in cataclastic areas (Scott et al. 1998). The study of Martian carbonates is important as these minerals precipitate from aqueous fluids and thus can be used to explore the history of water at the planet's surface and crust (Bridges et al. 2001; Tomkinson et al. 2013). Carbonate outcrops have been found on the Martian surface by orbiters, landers, and rovers (Bandfield et al. 2003; Ehlmann et al. 2008; Boynton et al. 2009; Morris et al. 2010). Carbonate deposits that may represent sites of paleolakes support the idea that Mars had a warmer and wetter past (Wray et al. 2011). In particular, the amount of carbonates present at the surface are a powerful tool for understanding the duration of the warmer and wetter period of Martian history. Additionally, carbonates can contain microstructures that form by high shock pressures and temperatures, thus enabling them to be used to explore the magnitude and frequency of impact events (Treiman 1998).

The carbonates in ALH 84001 are known to be Martian because they are cut by and predate some of the fractures mentioned previously, and so have received considerable attention. The detailed study by Corrigan and Harvey (2004) described them as "rosettes" (here termed "globules"), planiform "slabs," "post-slab" magnesites, and as interstitial carbonates, but they have been classified in several other ways (e.g., Saxton et al. 1998; Scott et al. 1998; Holland et al. 1999; Corrigan et al. 2003; Niles et al. 2005; Meyer [2012] and references therein). One early interpretation of their origin was that it was associated with early biologic activity on Mars (McKay et al. 1996), but subsequent studies have shown that their precipitation can also be explained by abiotic processes (Scott et al. 1998; Warren 1998; Golden et al. 2001; Treiman et al. 2002; Corrigan and Harvey 2004; Niles et al. 2006, 2009; Steele et al. 2007; Martel et al. 2012; Meyer [2012] and references therein). However, what make these carbonates objectively interesting are their formation process and their ~3.9 Gyr age (calculated using  $^{87}\text{Rb}$ - $^{86}\text{Sr}$  chronometry by Borg et al. 1999). The anomalies in magnetization of these carbonates could indicate that the Martian magnetic field shut off between the formation of these carbonates and the transition from the late Noachian to Hesperian (Weiss et al. 2002). ALH 84001 is not the only Martian meteorite containing carbonates, since they have also been described from the nakhlites (e.g., Carr et al. 1985; Chatzitheodoridis and Turner 1990; Bridges and Grady 2000; Bridges and Schwenzer 2012; Tomkinson et al. 2013). However, and although the formation process for those carbonate could be fairly similar (Bridges and Grady 2000; Bridges et al. 2001), their petrography and composition are clearly different (Lee et al. 2013;

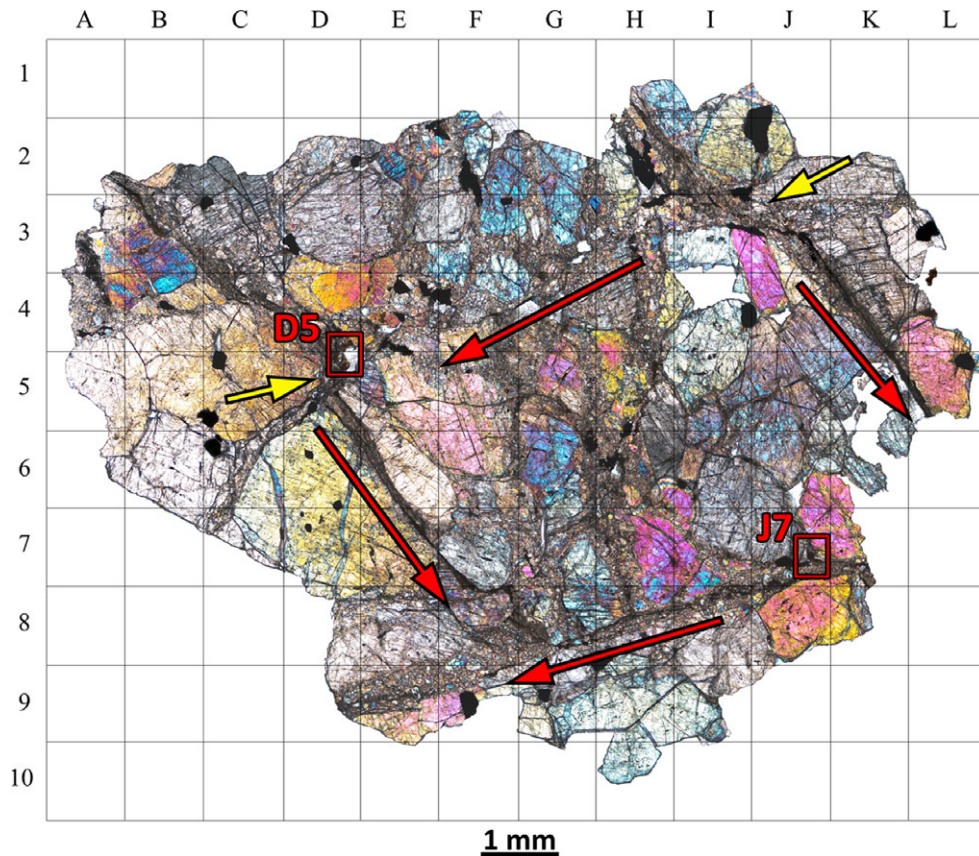


Fig. 1. High-resolution mosaic of the ALH 84001,82 thin section (images acquired in TL between crossed polarizers). Red arrows show the orientations of the two main fracture systems. Yellow arrows point to where the fractures intersect. Fractures oriented NNW-SSE are displaced by those aligned ENE-WSW. D5 and J7 are the two carbonate-containing regions studied.

Tomkinson et al. 2013). This is why we focus here on the study of the carbonates in ALH 84001, since they are much older and, therefore, provide information about the conditions on Mars long before the carbonates found on nakhlites were formed (Bridges et al. 2001).

The distribution of carbonates throughout ALH 84001 provides clues about the environmental conditions under which they formed, and can help to establish a link to the carbonates that have been found at the surface of Mars. Following several studies, two main formation scenarios at ~3.9 Gyr have been proposed (1) precipitation at low temperature (e.g., Romanek et al. 1995; Treiman 1995; McKay et al. 1996; Valley et al. 1997; Golden et al. 2000; Eiler et al. 2002; Theis et al. 2008; Halevy et al. 2011) and (2) precipitation from a fluid with high concentrations of CO<sub>2</sub>, possibly over a short time, at high temperatures (e.g., Mittlefehldt 1994; Harvey and McSween 1996; Scott et al. 1997a, 1998). This second scenario may have been the consequence of an impact event and subsequent hydrothermal activity (Harvey and McSween 1996; Treiman et al. 2002), or crystallization of shock-melted material (Scott et al.

1997a, 1998). The terrestrial carbonates described in Treiman et al. (2002) support, by analogy, formation because of Martian hydrothermal processes. Indeed, the carbonates found in ALH 84001 are compositionally different from the common carbonates (or any of their solid solutions) found on Earth. In fact, there are just a few regions on Earth where similar (but not identical) carbonates occur (Treiman et al. 2002), and they are out of the range of terrestrial carbonate solids solutions. Also, our studies provide complementary information for the multigenerational carbonate model that was described by previous authors (e.g., Corrigan and Harvey 2004). Our results provide textural and compositional evidence for precipitation of the carbonates by at least two different fluids.

## EXPERIMENTAL TECHNIQUES

ALH 84001 was found in the Far Western Icefield of Allan Hills by the Antarctic Search for Meteorites (ANSMET) program in 1984. A preliminary study provided a weathering degree of A/B and a “fracturing



category” of B (equivalent to an S4-5 shock grade of the classification used currently) (Score and MacPherson 1985). The NASA Johnson Space Center (JSC), responsible for the curation of the ANSMET collection, provided the 30  $\mu\text{m}$  thin section ALH 84001,82 (see Meyer [2012] for the specific location of this sample in the original rock). To comprehensively characterize carbonates in this sample we have used transmitted light (TL) and cathodoluminescence (CL) microscopy, electron microprobe analysis, micro-Raman spectroscopy, scanning electron microscopy (SEM), and energy-dispersive X-ray spectroscopy (EDS). The reasons why we have chosen each technique and its particular relevance to this study are explained below.

### **Petrographic Microscopy**

We used three petrographic microscopes. At the Institute of Space Sciences we worked with a Zeiss Scope, with magnifications up to 500 $\times$ , and with a Motic BA310Pol Binocular microscope (Motic, Hong Kong), which has a rotating platen that enables viewing of features including undulatory extinction. Both can work with crossed nicols. The third microscope, at the Universidad Complutense de Madrid, is a Nikon Eclipse LV100NPol (Nikon, Tokyo, Japan), working with magnifications up to 600 $\times$ . Summing the capabilities of the three of them we are able to work with reflected light (RL), transmitted light (TL, particularly useful to recognize features on samples with a size of tens of  $\mu\text{m}$ ), TL under crossed nicols (for identifying minerals), and with bright field (high contrast and differentiation between more and less dense materials), or dark field illumination (use of scattered light to increase the visibility of low relief features). These techniques enable a great deal of information to be obtained from the regions of interest. We used these microscopes to take 500 $\times$  images of the ALH 84001, 82 sections. To have a reference map we merged the TL images in a high-resolution mosaic (Fig. 1). A grid was superimposed to the image (square size is 1  $\text{mm}^2$ ) to easily navigate around the section and so (re)locate regions of interest.

### **Cathodoluminescence Microscopy**

With regard to CL, the light emitted during electron bombardment of a mineral has an intensity and wavelength that depends on its chemical composition and crystallographic structure (Burns 1969). Even trace amounts of some elements can act as activators or quenchers of CL (Götze et al. 2000; Akridge et al. 2004). The energy of the electron beam can also have an influence on CL emission (Akridge et al. 2004).

Therefore, to correctly interpret CL results it is important to constrain the mineralogy of the sample being studied. Iron-free minerals can be particularly luminescent, as iron is a typical quencher (Burns 1969). With this property in mind, carbonates can be identified in the thin section as they are zoned, with layers that are Mg-rich and Fe-free (Saxton et al. 1998), which should luminesce red (Akridge et al. 2004). In this study, we used a Technosyn cold cathodoluminescent MK4 (Cambridge Image Technology Ltd., Welwyn Garden City, UK) operated at 20–24 kV/350–400 mA, at the Universidad Complutense de Madrid. The CL was used to create a mosaic of the thin section together with higher magnification and resolution images (Fig. S1 in supporting information and Fig. 2).

### **Scanning Electron Microscopy**

Two SEMs were used: a FEI Quanta 650 FEG (FEI, Hillsboro, Oregon, USA) with a back-scattered electron detector (BSED), at the Institut Català de Nanociència i Nanotecnologia (ICN2), and a JEOL JSM7600F at the National Center for Electron Microscopy (ICTS) at the Universidad Complutense de Madrid. The Quanta 650 was operated in low-vacuum mode with the thin section uncoated so that any carbon detected by EDS analysis was not from the coating. Secondary electron (SE) and Back-scattered electron (BSE) imaging was used to study in detail sites of interest in the sample, and at magnifications of up to 27,000 $\times$  (see Figs. 3–6). The SEM was also used to select regions and points of interest for subsequent chemical analysis by electron microprobe.

### **Energy-Dispersive X-ray Spectroscopy**

EDS was used to create elemental maps of the regions of interest (Fig. 3). The EDS detector was an Inca 250 SSD XMax20 (Oxford Instruments, Abingdon, UK) with a detector area of 20  $\text{mm}^2$ , attached to the SEM at the Institut Català de Nanociència i Nanotecnologia (ICN2). Since we had available the electron microprobe technique, EDS was mostly used to create the illustrative chemical maps (Fig. 3), instead of performing quantitative chemical analyses. The accelerating voltages were 20 kV and the totals were normalized to 100%.

### **Micro-Raman Spectroscopy**

Micro-Raman spectra were acquired from the carbonates using a Jobin-Yvon T-64,000 Raman spectrometer (HORIBA Ltd., Kyoto, Japan) at the Institut de Ciència de Materials de Barcelona (ICMAB-

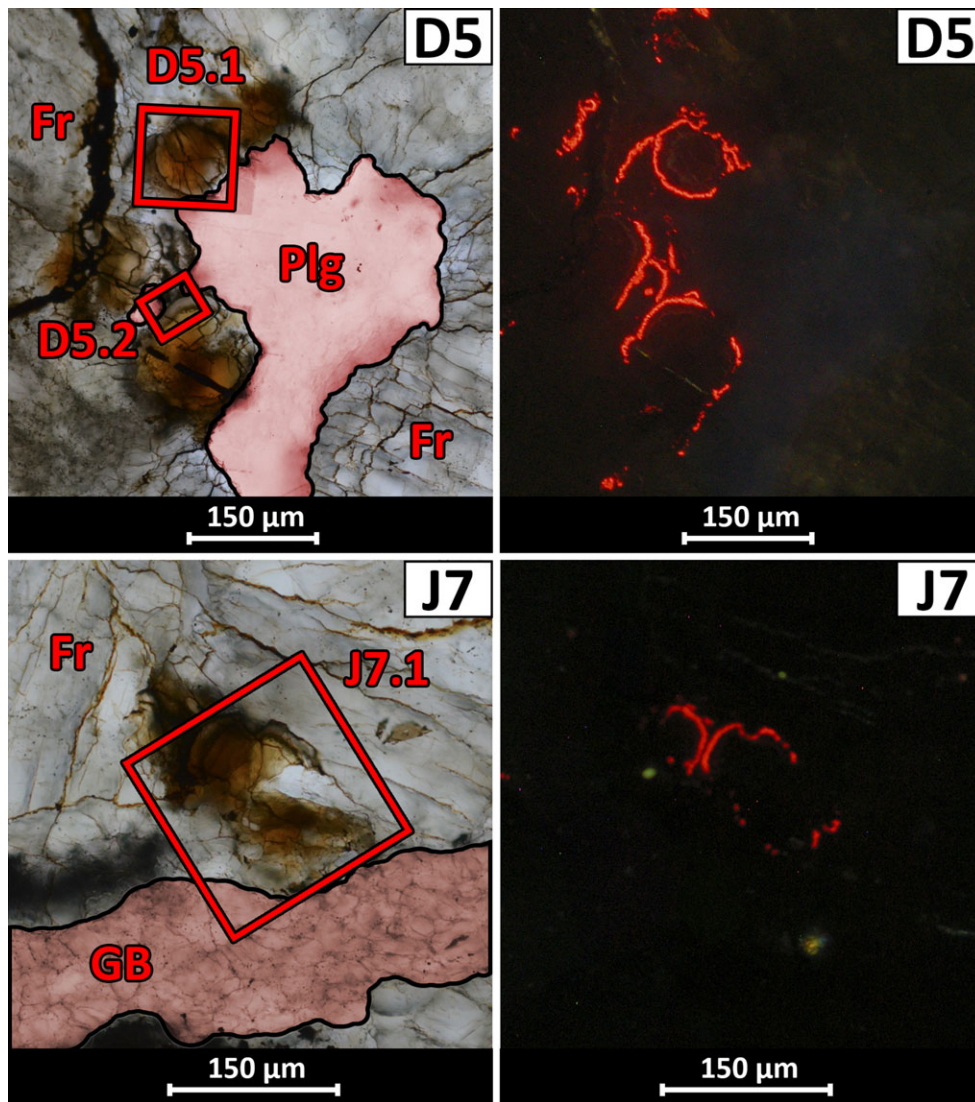


Fig. 2. Detail of the two regions of interest highlighted in Fig. 1 and S1 (D5 and J7); TL left, CL right. Carbonates are the brown to orange areas in TL, while their Fe-poor and Mn-rich layers are the red rims in CL. In the TL images we draw attention to the fractures around regions where the carbonates are present (Fr). The maskelynite or shock-modified plagioclase glass solidified in a fracture or pore after formation of the carbonates at D5 (Plg, highlighted in red), and in one of the so-called granular bands (Mittlefehldt 1997) next to the carbonate at J7 (GB, painted in red). Three areas that are in some of the later Figures (D5.1 and J7.1) are also highlighted.

CSIC). The instrument was attached to an Olympus microscope and equipped with a liquid nitrogen-cooled CCD detector, and was operated in backscattering geometry at room temperature using the 5145 Å line of an argon-ion laser. The lateral spatial resolution was  $\sim 1 \mu\text{m}$ , and the laser power onto the sample was maintained between 0.6 and 0.7 mW to avoid degradation or excessive heating. High-resolution spectra were acquired in working windows between 100 and  $1400 \text{ cm}^{-1}$ . The instrument was used to better characterize the composition of the carbonates and possibly also to detect shock features (Fig. 4).

#### Electron Microprobe

Quantitative chemical analyses and BSE images were obtained using a JEOL JXA-8900 electron microprobe (JEOL Ltd., Tokyo, Japan) equipped with five wavelength-dispersive spectrometers at the Universidad Complutense de Madrid.

More than 160 spot analyses were acquired from the carbonate globules (Fig. 5) using an accelerating voltage of 15 kV, beam current of 10 nA, and a spot size of  $1 \mu\text{m}$ ; line profiles used 15 kV/100 nA, and spot size and step interval of  $1 \mu\text{m}$  diameter (dwell time = 1000 msec).



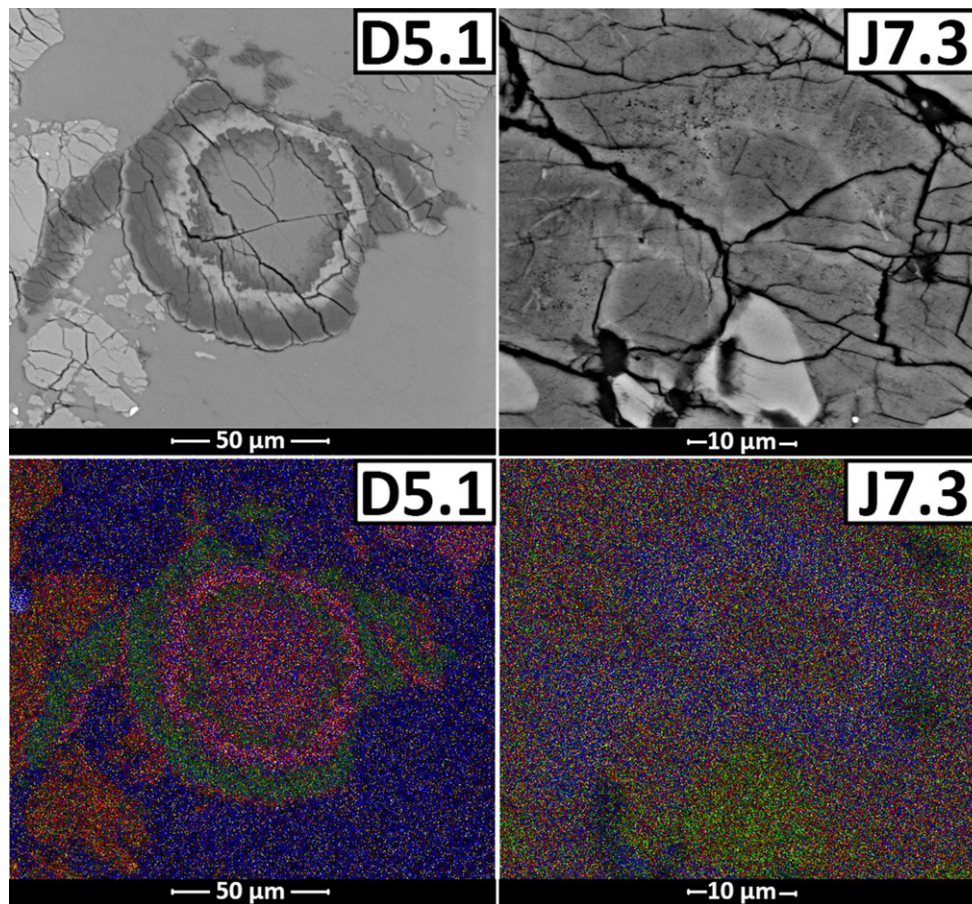


Fig. 3. BSE images of the areas D5.1 and J7.3 (see Figs. 2 and 4 for the location of J7.3) with corresponding EDS maps revealing the distribution of Ca (blue), Fe (red), Mg (green), and Mn (yellow). In D5.1, the Fe-rich and Mg-rich rims of the carbonate can be clearly observed. Also note that the outer layers of the globules are partially corroded, and that the surrounding mineral (maskelynite, or shock-modified plagioclase) incorporates fragments of the carbonate. In J7.3, the carbonate is compositionally more homogeneous, apart from the outermost part of layer #2 (see J7.3 in Fig. 7), whose Ca-rich composition is shown more clearly by the EDS map than by the BSE image.

The counting time for spot analyses was 30 s per element, although 5 elements could be analyzed simultaneously. The relatively low voltage, beam current, and counting time employed for the carbonate spot analyses minimized beam damage. The standards used were siderite for Fe and Mn, and dolomite for Mg and Ca. Measured precision was better than  $\pm 0.0014\%$  for Mg,  $\pm 0.009\%$  for Ca,  $\pm 0.005\%$  for Fe, and  $\pm 0.19\%$  for Mn. Detection limits were 150–180 ppm for Mg, 150–200 ppm for Ca, 350–500 ppm for Fe, and 400–510 ppm for Mn. Elemental compositions were given as element oxides % and were recalculated to mol% of  $\text{MgCO}_3$ ,  $\text{CaCO}_3$ ,  $\text{FeCO}_3$ , and  $\text{MnCO}_3$ .

## RESULTS

Our work has focused on carbonates in the regions marked D5 and J7 on the TL and CL high-resolution mosaics (Figs. 1 and 2 and S1). D5 contains abundant

carbonate globules attached to the walls of a former pore (Fig. 2), while J7 is a large globule that lies next to a granular band (Fig. 2), and has a rhombohedral core (J7.3 in Figs. 3–5 and 7). In these regions, both of which are close to fractured areas, the space between carbonate globules contains maskelynite, which has probably formed by shock transformation of plagioclase (Fig. 2).

### Petrographic Context and Microstructures of the Carbonates

Two main fracture orientations can be identified in Fig. 1; one is aligned NNW-SSE, and the other ENE-WSW. As the ENE-WSW fractures cross-cut and displace the other set, they must be younger (Fig. 1). CL imaging highlights some of the layers in carbonates by their high intensity of red luminescence in comparison to the rest of the sample (which is largely non-luminescent; Fig. S1). The high CL intensity is

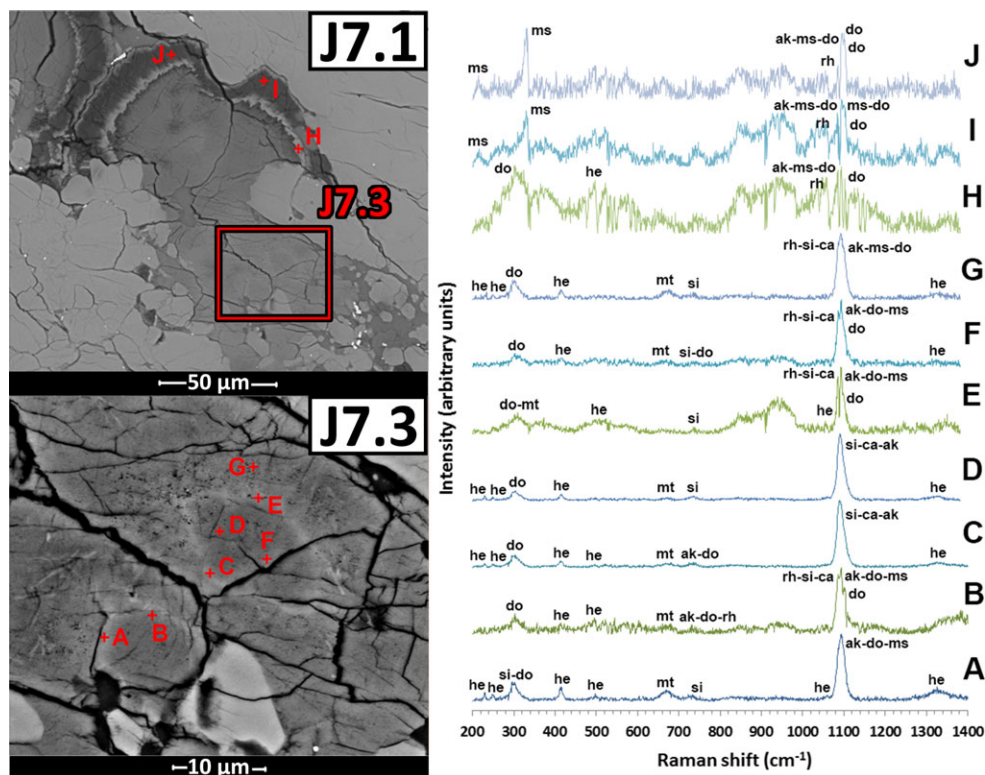


Fig. 4. BSE images of areas J7.1 and J7.3 (see Fig. 2), where Raman spectroscopy was performed (left) and corresponding Raman spectra (right). The minerals that match each peak have been suggested (according to the data in the RRUFF catalog; Downs 2006): ms (magnesite), ak (ankerite), do (dolomite), rh (rhodochrosite), he (hematite), mt (magnetite), si (siderite), ca (calcite). The positions of the peaks are listed in Table S1.

inferred to be the consequence of a particularly low content of Fe, which would otherwise quench the Mn-activated luminescence (e.g., Machel et al. 1991). Areas with blue to gray CL (pale areas under TL) are maskelynite or plagioclase glass (Plg in Fig. 2). Non-luminescent grains are chromite (a few can be seen in Fig. S1). As expected, we found that carbonates are present in or close to fractures, and are also dispersed throughout the matrix-breccia (Figs. 1 and 2 and S1). In regions where the two fracture systems cross-cut, globules seem to be bigger and more abundant (e.g., D5), and plagioclase is also more abundant (Figs. 1 and 2 and S1).

SEM work shows that the carbonate globules are characterized by a very clear and previously well-documented zonation that divides them into several “layers” (e.g., Saxton et al. 1998; Holland et al. 1999; Golden et al. 2001; Corrigan and Harvey 2004). This zoning can be readily characterized by BSE imaging (Figs. 3–6) and EDS element mapping (Fig. 3). The layers are differentiated using the scheme in Fig. 7. The pattern of layering is comparable between globules, although in J7 the oldest part can be recognized (J7.3 in Figs. 3–5 and 7). A preliminary description of this

“core” was provided by Moyano-Camero et al. (2014). It is likely to be equivalent to the central regions of other globules, but is surrounded by a thin rim that is lighter gray in BSE images (and therefore has a higher mean atomic number). The core has a rhombohedral shape, which is consistent with a carbonate mineral (i.e., calcite, siderite, magnesite, rhodochrosite, ankerite, or dolomite). Hereafter, we refer to the core and its rim as layers #1 and #2 respectively (see J7.3 in Fig. 7). Layer #2 is followed by a much thicker and uniform layer (#3) that is comparable to layer #1 in BSE images (see J7.6 in Figs. 6 and 7). Layer #3 is equivalent to the first-formed zone that has been distinguished in other globules found in this sample (e.g., D5.1 in Figs. 3–6), which we also call layer #3 (Fig. 7). Carbonate globules in the two selected areas (D5 and J7) gradually become darker in BSE images (lower in mean atomic number) until their euhedral terminations at the margins of layer #4 (Figs. 6 and 7). It is interesting to note the presence of small fractures that terminate at the end of layer #4 and do not affect layer #5 (Fig. 6). Also, we observed that although the boundary between layers #4 and #5 is mostly euhedral, in some areas, a small-scale corrosion can be observed affecting the outermost part of layer #4



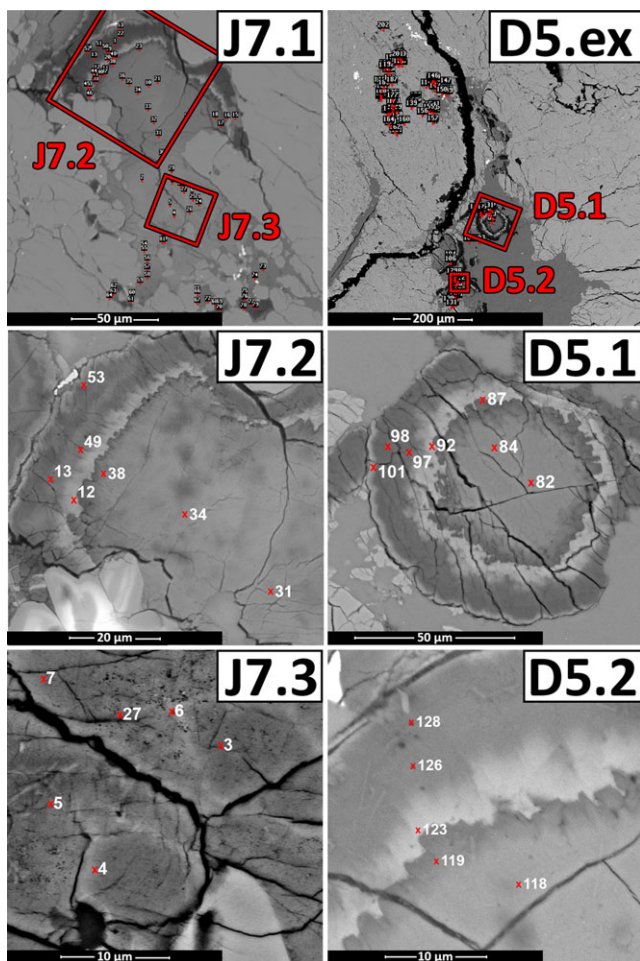


Fig. 5. BSE images of the carbonate globules studied, including the locations of the 160 microprobe spots. J7.1 is highlighted in Fig. 2, and J7.2 and J7.3 are showing detail of this area. D5.ex is a region showing D5 (see Figs. 1 and 2; Fig. S1) but also the area above, where some carbonates were analyzed. D5.1 and D5.2 are also showing specific areas in greater detail, and both were already highlighted in Fig. 2. All the data obtained are shown in Fig. 10. Only some example points can be seen in J7.2, J7.3, D5.1, and D5.2; the data obtained from these points are listed in Table 1.

(Fig. 6). Layer #5, distinctive in BSE images, gradually grades into layer #6, which has a lower mean atomic number. Finally, the zonation ends in a very thin and clear area (layer #7), although it is not present in all globules (Fig. 7). At the boundaries between layer #4 and #5, and between #6 and #7, are small inclusions of high atomic number, which are petrographically compatible with Fe oxides and sulfides (Fig. 6, D5.5). However, the very small size of these minerals (<500 nm) meant that we were unable to characterize them properly. Nevertheless, the areas containing these minerals have overall higher content of Fe than the surrounding carbonate, and lower concentrations of Na,

Cr and locally S (<1%), which are not detected in the surrounding carbonate.

### Carbonate and Oxide Mineralogy

The Raman spectrometer was used to analyze carbonate in J7 (Fig. 4). CrystalSleuth software (Laetsch and Downs 2006) was used to compare the spectra obtained with those in the RRUFF catalog (Downs 2006), and to remove the background from our spectra. As a consequence, the particularly fluorescent spectra obtained at points H, I, and J were very noisy, but interesting features could nonetheless be distinguished (Fig. 4). The main peaks obtained (Table S1 in supporting information) are not easily attributed to a specific carbonate mineral. As shown in Fig. 4 several minor peaks ( $\sim 230$ , 250, 300, 415, and  $1320\text{ cm}^{-1}$ ) can be related to hematite, which is consistent with previous studies suggesting the presence of microcrystalline grains of this mineral within the carbonates (Steele et al. 2007). The peak that occurs in all the spectra at  $\sim 300\text{ cm}^{-1}$ , which is common in carbonates but varies with composition, can be modified by one peak of hematite existing at approximately the same wavenumber. Therefore, and although in most cases they seem similar to the dolomite peak, we cannot truly associate the exact position of this peak to that of a specific carbonate mineral (except for I and J, where the typical  $330\text{ cm}^{-1}$  peak of magnesite can be clearly recognized). The peak at  $\sim 730\text{ cm}^{-1}$  also proved to be difficult to attribute, as most spectra show Raman shifts that are too high compared with the common values for carbonates. This is why in Fig. 4 those peaks are mainly associated with siderite, because it is the carbonate showing a highest shift for this peak. Something similar happens with the peak at  $\sim 1100\text{ cm}^{-1}$ . Apart from a minor possible influence of hematite in the peak position, all the analyzed points (apart from A, C, and D) show between 2 and 4 peaks in the  $1085\text{--}1103\text{ cm}^{-1}$  region (Table S1). Also of interest is a peak at between  $660$  and  $680\text{ cm}^{-1}$  that can be clearly distinguished in several of the spectra (Fig. 4) and is interpreted to indicate the presence of magnetite, whose most prominent peak is at  $\sim 660\text{ cm}^{-1}$ . This finding of magnetite is consistent with previous studies (McKay et al. 1996; Cooney et al. 1999), although according to our Raman results it seems to be present all around the carbonate at J7 (Fig. 4), and presumably in other carbonates too.

### Carbonate Compositional Zoning

EDS element maps of D5.1 (Fig. 3) show the alternating Fe-rich (red) and Mg-rich (green) nature of



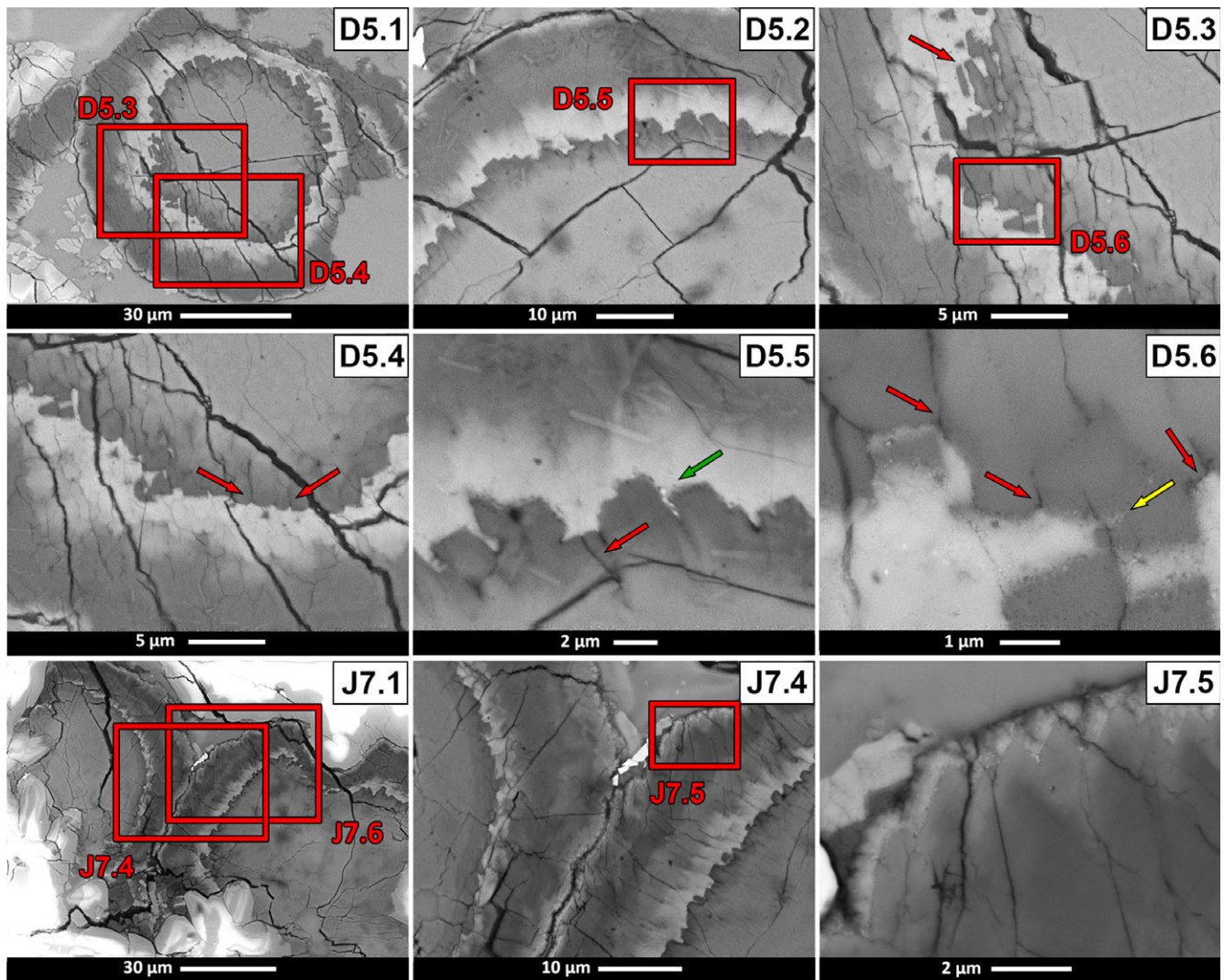


Fig. 6. Detailed BSE images showing the boundary features between layers #4 and #5 (D5.1-D5.6) on carbonate globules (see also D5.1 in Fig. 7). Red arrows point to the small fractures that terminate at the end of layer #4. The green arrow indicates small high atomic number inclusions. The yellow arrow shows corrosion at the end of layer #4. J7.1, J7.4, and J7.5 show the complex gradation in color (and composition) between layers #5 and #7 (see J7.6 in Fig. 7).

the layers. Electron microprobe analyses were used to quantify carbonate chemistry at ~160 points in the sample (Fig. 5) and show the progressive compositional trends in the globules. The overall composition of each layer is given in Table S1 and the microprobe profiles and spot analyses of globules D5 and J7 are in Figs. 8 and 9, respectively. A subset of these data (the spots marked at J7.2, J7.3, D5.1, and D5.2 in Fig. 5) are listed in Table 1.

Layers #1 and #2, are visible only in the carbonate at J7 (points 3, 4, and 6 at J7.3). They differ from other zones in having intermediate concentrations of Fe and Mg, and the highest Ca compositions, plus relatively high Mn values (Figs. 8 and 9; Table 2). The main

differences between the two layers are that #2 has a lower Mg, and greater Ca, Mn, and Fe concentrations. The outer part of layer #2 (indicated as “outer #2” in Fig. 7) shows high Ca and Mn compared with any other regions in the carbonates, and simultaneously very low Fe and Mg abundances (Figs. 8 and 9; Table 2, and points 27 and 5 at J7.3 in Fig. 5; Table 1). This specific portion of layer #2 cannot be clearly resolved in BSE images, but can be easily identified as a blue ring (Ca-rich region) in the elemental map at J7.3 (Fig. 3). Layer #3 is characterized by a progressive decrease in Ca, Mn, and Fe with a concomitant enrichment in Mg (Figs. 8 and 9; Table 2; see points 7, 31, 34, 82, 84, and 118 in Fig. 5; Table 1). We have

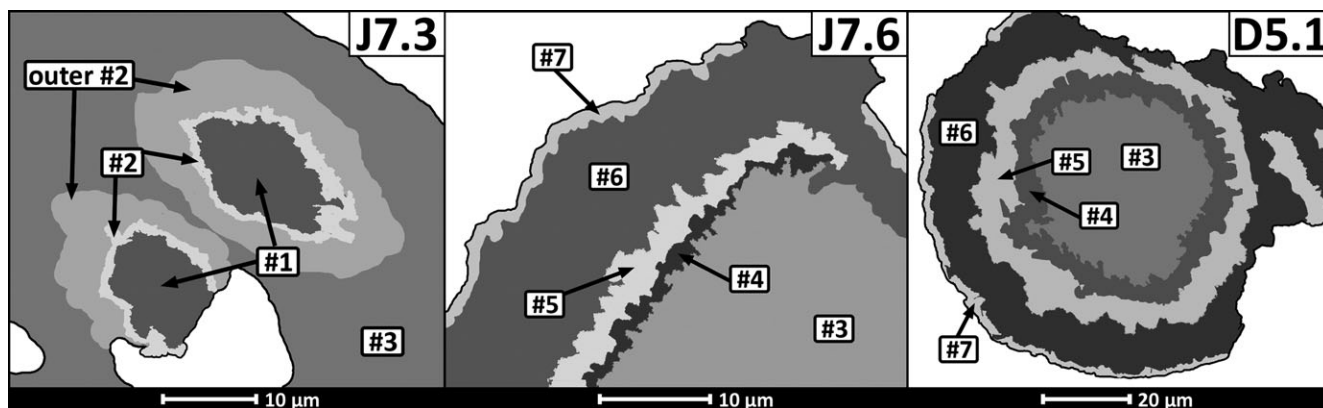


Fig. 7. Schematic images showing the different layers in the carbonates studied. The area indicated as “outer #2” is the portion of layer #2 that is distinguishable as a blue ring in the element map (Fig. 3).

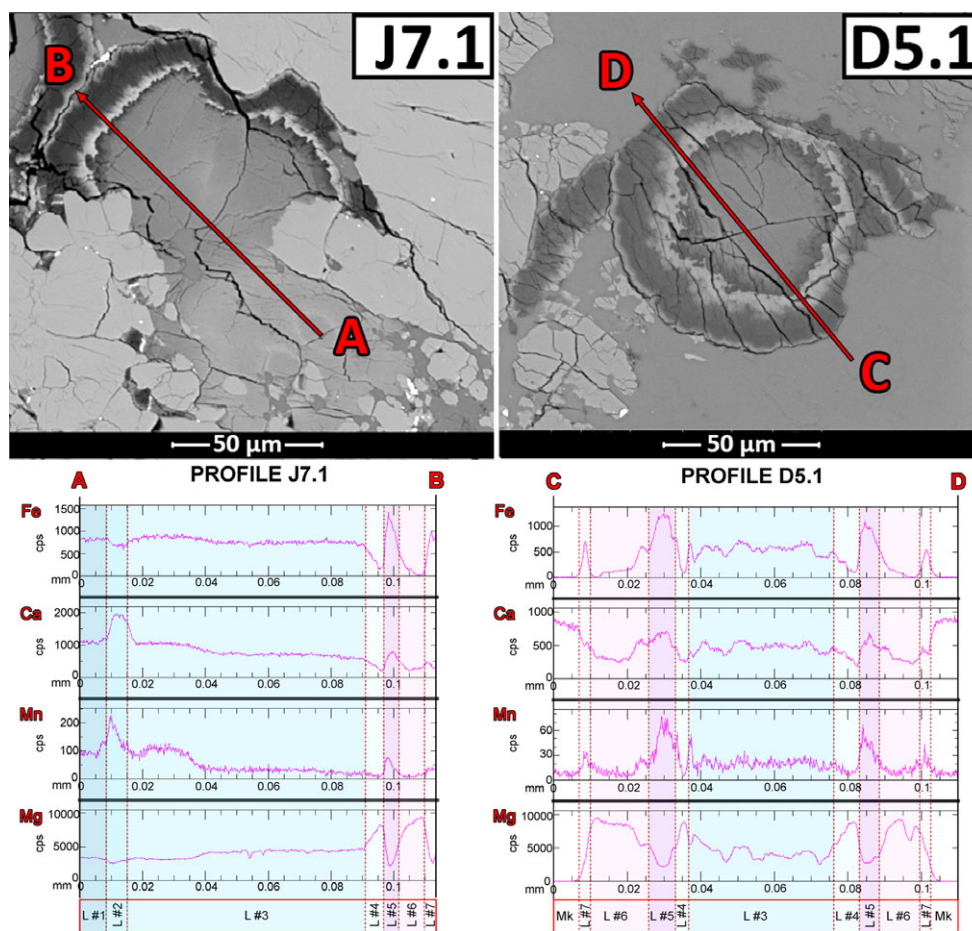


Fig. 8. Elemental profiles obtained by electron microprobe showing progressive geochemical variations along two globules. In the upper part, the lines along which the profiles were obtained are indicated, in J7.1 and D5.1. Cps: counts per second; L: layer; Mk: maskelynite (or shock-modified plagioclase glass).

divided this compositional progression in three phases: #3.1 (the closest area to layer #2, still quite Ca- and Mn-rich), #3.2 (main layer #3, the wide area between

layers #2 and #4), and #3.3 (the closest area to layer #4). Layer #4 (like in points 38, 87, and 119, Fig. 5) follows the variation in composition started in layer #3

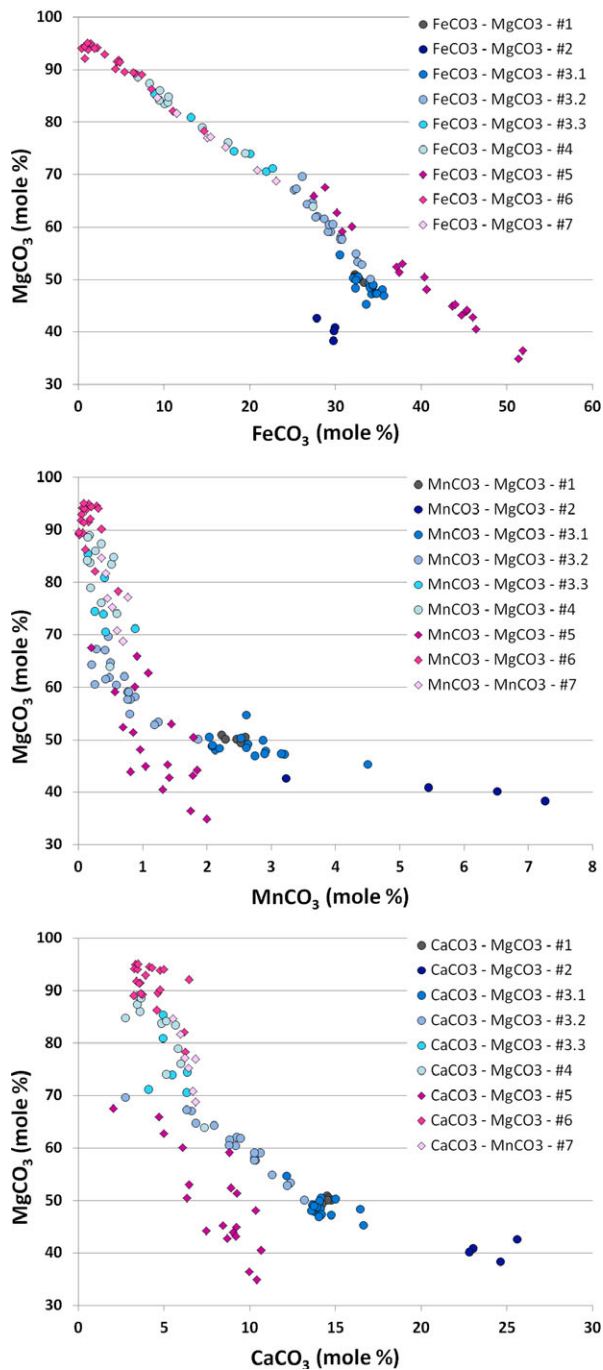


Fig. 9. Plots of  $\text{MgCO}_3$  versus  $\text{FeCO}_3$ ,  $\text{MnCO}_3$  and  $\text{CaCO}_3$  (in mole%) derived from microprobe analyses (see J7.1 and D5.ex in Fig. 5). Each layer is marked with a different color. Also, layers #1 and #4 (before the euhedral shape), are represented by bluish circles, while layers #5 to #7 are represented by purple to pink diamonds. As compositions vary within layer #3 (see Fig. 7), it is subdivided into #3.1 (slightly clearer, just after layer #2), #3.2 (intermediate between layers #2 and #4) and #3.3 (slightly darker, just before layer #4).

but at greater intensity, until reaching very high contents in Mg (Figs. 8 and 9). Layer #5 shows an abrupt change in globule composition compared with layer #4 (Figs. 9 and 10); Mg content strongly decreases whereas Fe, Ca, and Mn concomitantly increase (Figs. 9 and 10; points 12, 92, and 123, Fig. 5). This sharp change in carbonate composition coincides with the presence of local corrosion and the small fractures affecting the end of layer #4 and not affecting layer #5 (Fig. 6). In layer #6 (points 49, 13, 97, 98, 126, and 128, Fig. 5), there is again a progression toward a very Mg-rich carbonate (Figs. 8 and 9; points 98 and 128 in Fig. 5; Table 2). This layer has the lowest Fe contents, thus accounting for its high luminescence intensity. Some globules have a thin Fe, Ca, and Mn-rich rim (layer #7, represented by point 101, Fig. 5) which exhibits higher Fe, Ca, and Mn contents than layer #6 (Figs. 8 and 9).

The microprobe data were plotted in a ternary diagram (Fig. 10) for comparison with the results of previous studies, with terrestrial carbonates, and with the distribution of carbonate solid solutions (Chang et al. 1996). According to the ternary diagrams (Fig. 10), the studied carbonates are not in the range of terrestrial carbonate solid solutions, and have a composition that is intermediate between dolomite, ankerite, and the siderite-magnesite solid solutions. The carbonates studied here are compositionally similar to those analyzed by previous authors (Mittlefehldt 1994; Harvey and McSween 1996; Valley et al. 1997; Scott et al. 1998; Holland et al. 1999, 2005; Eiler et al. 2002; Corrigan and Harvey 2004; Halevy et al. 2011), as shown in Fig. 10. However, some of those authors observed a very Ca-rich carbonate phase in bulk samples of ALH 84001, and in thin sections ALH 84001,119, ALH 84001,287, ALH 84001,302, and ALH 84001,303, which is not observed in the sample studied here, ALH 84001,82.

## DISCUSSION

### Environment of Carbonate Precipitation

It has been suggested that most of the ALH 84001 carbonates formed from a  $\text{CO}_2$ -enriched aqueous fluid penetrating an already brecciated rock (Harvey and McSween 1996). These processes are interpreted to have coincided with impact metamorphism, perhaps with the solutions sourced from a transient impact crater lake (Warren 1998). Formation of the carbonate in a low-temperature near-surface environment over short timescales has been suggested (Berk et al. 2010), maybe by a mixture of subsurface and atmosphere-derived



Table 1. Chemical compositions obtained from the carbonate globule analyses in Fig. 5.

Point	Layer	MgCO <sub>3</sub>	FeCO <sub>3</sub>	CaCO <sub>3</sub>	MnCO <sub>3</sub>
31 (J7.2)	#3	57.91	30.89	10.38	0.81
34 (J7.2)	#3	57.86	31.04	10.33	0.77
38 (J7.2)	#3	71.00	22.19	6.38	0.43
12 (J7.2)	#5	36.21	52.07	9.97	1.75
49 (J7.2)	#6	89.26	7.46	3.26	0.01
13 (J7.2)	#6	91.80	4.75	3.41	0.04
53 (J7.2)	#7	81.94	11.62	6.01	0.43
3 (J7.3)	#1	50.80	32.43	14.53	2.23
4 (J7.3)	#1	50.41	32.38	14.60	2.60
6 (J7.3)	#2	45.18	33.68	16.63	4.52
27 (J7.3)	#2	40.31	30.15	22.96	6.58
5 (J7.3)	#2	38.21	29.86	24.64	7.29
7 (J7.3)	#3	50.20	32.25	15.01	2.53
82 (D5.1)	#3	60.86	30.02	8.87	0.25
84 (D5.1)	#3	66.24	25.95	7.26	0.54
87 (D5.1)	#4	87.79	8.39	3.46	0.35
92 (D5.1)	#5	60.49	32.45	6.17	0.89
97 (D5.1)	#6	86.65	8.62	4.62	0.11
98 (D5.1)	#6	93.96	1.11	4.79	0.13
101 (D5.1)	#7	77.37	15.58	6.27	0.77
118 (D5.2)	#3	65.34	27.21	7.05	0.40
119 (D5.2)	#4	85.06	9.61	5.19	0.14
123 (D5.2)	#5	43.46	45.43	9.31	1.80
126 (D5.2)	#6	91.49	4.86	3.56	0.09
128 (D5.2)	#6	92.51	0.78	6.52	0.19

Data obtained by electron microprobe.

The values are mole% carbonates.

fluids or within an alkaline spring environment (Niles et al. 2005; Halevy et al. 2011). Similar carbonates have been found only in a few places in Earth, and the presence of magnesite rather than hydromagnesite, the C and O isotope ratios consistent with near-surface reservoirs and ocean water, respectively, and the lack of uniformity in the distribution of carbonates, point toward a hydrothermal origin for them (Treiman et al. 2002). Because of the similarities between these terrestrial carbonates and those in ALH 84001, an origin in a hydrothermal system has been proposed (Treiman et al. 2002).

### Relative Chronology of Carbonate Precipitation

There have been several interpretations of the proposed ages of these carbonates (Nyquist et al. 2001), and the present study suggests that different types, and maybe different generations, are present (Mittlefehldt 1994). According to our petrographic and geochemical results, the formation of these carbonates can be divided into at least two phases of precipitation. The carbonates precipitated in this meteorite as zoned globules, disks, or slabs along fractures, and as

interstitial material within pyroxene crystals (e.g., Corrigan et al. 2003; Corrigan and Harvey 2004). In the studied section, carbonate globules are found mostly in regions that had been previously highly fractured (Figs. 1 and 2 and S1), like the points where the two fracture systems intersect. The presence of these distinct fracture systems, with the one aligned NNW-SSE being traversed and displaced by the one aligned ENE-WSW, suggests that the sample also experienced at least two shock events. Granular bands (i.e., “GB” in Fig. 2), have been previously interpreted as being older than the fractures (Mittlefehldt 1997), pointing toward more than two shock events. However, we consider the granular bands to be contemporary with the fractures. Indeed, these types of bands typically form as a product of friction during terrestrial fracturing (see e.g., Brodie et al. 2007, where they are named cataclasites). These bands could actually show a high carbonate content owing to their greater original porosity.

In common with previous models (e.g., Schwandt et al. 1999), we suggest that the most plausible scenario for carbonate formation is initial precipitation from Mg- and Fe-rich solutions, followed by the formation of maskelynite or shock-modified plagioclase glass (Fig. 2) during a shock event (Mittlefehldt 1994; Treiman 1995, 1998; Scott et al. 1997b; Cooney et al. 1999; Greenwood and McSween 2001; Corrigan et al. 2003). These solutions would have filled the shock-produced fractures at different times, leading to the precipitation of carbonates in at least two events. Indeed, carbonates are partially corroded at their contact with maskelynite or plagioclase glass (Fig. 3, D5.1). The density of fractures also differs dramatically between the carbonate and glass (Mittlefehldt 1994), which supports the suggestion that out of these two components the carbonates formed first. The presence of these solutions, along with other evidence (described, e.g., in Niles et al. [2006] and references therein) imply that liquid water was relatively abundant on Mars ~3.9 Gyr ago. In fact, those carbonates could be just a small sample of the products of quite a common phenomenon on the subsurface of Mars (Michalski and Niles 2010).

The characteristic compositional zoning of ALH840001 carbonates (e.g., Saxton et al. 1998; Corrigan and Harvey 2004) indicates that they precipitated in a manner whereby each zone formed when saturation was reached (Halevy et al. 2011). This zonation has been described as a consequence of chemical variation of their parent fluid, driven by the carbonate precipitation since Fe-, Mn-, and Ca-rich solutions are more kinetically favored to precipitate than Mg-rich solutions (Harvey and McSween 1996; Saxton et al. 1998; Corrigan et al. 2003; Corrigan and Harvey 2004; Niles

Table 2. Mean and range in chemical composition (maximum and minimum values) for the globule layers.

Layer	<i>n</i>	MgCO <sub>3</sub>		FeCO <sub>3</sub>		CaCO <sub>3</sub>		MnCO <sub>3</sub>	
		Mean	Range	Mean	Range	Mean	Range	Mean	Range
1	5	50.3	50.9–49.5	32.5	33.3–32.2	14.5	14.7–14.2	2.4	2.6–2.2
2	4	40.6	42.7–38.4	29.3	29.9–27.8	24.0	25.6–22.8	5.6	7.3–3.2
3.1	16	48.8	54.8–45.4	33.7	35.6–30.5	14.2	16.6–12.1	2.7	4.5–2.0
3.2	25	61.0	71.6–50.2	28.7	34.0–20.5	9.1	13.2–2.7	0.7	1.9–0.2
3.3	7	77.1	85.5–70.6	16.9	22.6–8.8	5.0	6.3–3.0	0.4	0.9–0.2
4	12	81.7	89.1–64.0	12.5	27.3–6.8	4.7	7.4–2.7	0.3	0.6–0.1
5	19	49.8	67.5–35.0	40.1	51.9–27.4	7.9	10.7–2.0	1.2	2–0.2
6	21	90.9	95.1–78.3	4.4	14.7–0.3	4.3	6.5–3.2	0.2	0.6–0.0
7	7	76.5	84.7–68.8	16.0	23.1–9.2	6.3	6.8–5.5	0.5	0.8–0.4

Data obtained by electron microprobe.

The values are mole% carbonates.

*n* = number of analyses.

et al. 2009; among others). The last carbonates to precipitate are therefore Mg-rich, only when the initial fluid is much more depleted in Fe, Ca, and Mn than it was at the beginning. Despite other differences, this zonation is equivalent between the globules and the interstitial carbonates precipitated within pyroxene crystals (see e.g., Scott et al. [1998] for the distinction between carbonates). A similar trend in the chemical evolution of the carbonates can be observed twice (from layers #1 to #4, and from #5 to #6) (Figs. 9 and 10), which together with evidence described later suggests that these carbonates precipitated in at least two events.

### Carbonate Mineralogy

None of the carbonate spectra in the RRUFF database precisely fit any of our Raman results. This finding, together with the multiplicity of peaks and the clear asymmetry of some of them (Fig. 4 and Table S1), could suggest that the ALH 84001 carbonates are a mixture of several phases, or compositionally heterogeneous on the submicroscopic scale (Cooney et al. 1999). However, our results suggest the presence of a single and compositionally unusual mineral with varying compositions, like the carbonates described by Treiman et al. (2002). This phase has yet to be properly characterized, and doing so will require further work using techniques such as X-ray diffraction and transmission electron microscopy. Raman spectroscopy has demonstrated the presence of hematite and magnetite in those carbonates that were analyzed for the present study (Fig. 4). Hematite affects the positions of several carbonate peaks, and therefore should be taken into account carefully when studying ALH 84001. The presence of magnetite, whose most prominent peak lies at  $\sim 660\text{ cm}^{-1}$ , is consistent with the results of previous studies (McKay et al. 1996; Cooney et al.

1999), although it seems to be present throughout these carbonates (Fig. 4).

As previously noted, our evidence suggests that ALH 84001 carbonates precipitated in at least two different episodes. Consistently, the fracturing and local corrosion of the euhedral crystals of layer #4 prior to precipitation of layer #5 (Fig. 6, D5.3-D5.6) indicate that layers #1 to #4 correspond to the first stage of precipitation, while layers #5 to #7 formed in the second stage and as an overgrowth. Moreover, the sharp transition in carbonate compositions between #4 and #5 suggests a change in solution chemistry and saturation state (e.g., the concentration in CO<sub>2</sub> or pH), between formation of the inner (#1 to #4) and outer (#5 to #7) layers. The microprobe data reveal two trends (Figs. 9 and 10) that add further weight to the idea of at least two episodes of precipitation. Indeed, the contrasting compositional trends imply that the ambient fluids differed in chemistry, pointing to distinct aqueous alteration events (Fig. 6). The distribution coefficients for Fe and Mn into carbonates are much higher than 1, meaning that any Fe<sup>2+</sup> or Mn<sup>2+</sup> in the fluid will preferentially partition into the carbonate (e.g., Chang et al. 1996; Rimstidt et al. 1998). Moreover, the distribution coefficients are not strongly temperature-dependent because of the fact that all solubility products of carbonate minerals change with temperature in almost the same way, at least between 273 and 373 K (Rimstidt et al. 1998). Assuming that the system was closed so that the aqueous solutions were not being continually replenished, Fe and Mn would progressively be depleted relative to Mg as carbonate precipitated from this fluid. This process may be responsible for the chemical patterns observed between layers #2 to #4 and layers #5 to #6 (Figs. 9 and 10). Layer #1 probably represents an initial precipitation, from a relatively Mg- and Fe-rich fluid. Once the concentration on Fe became

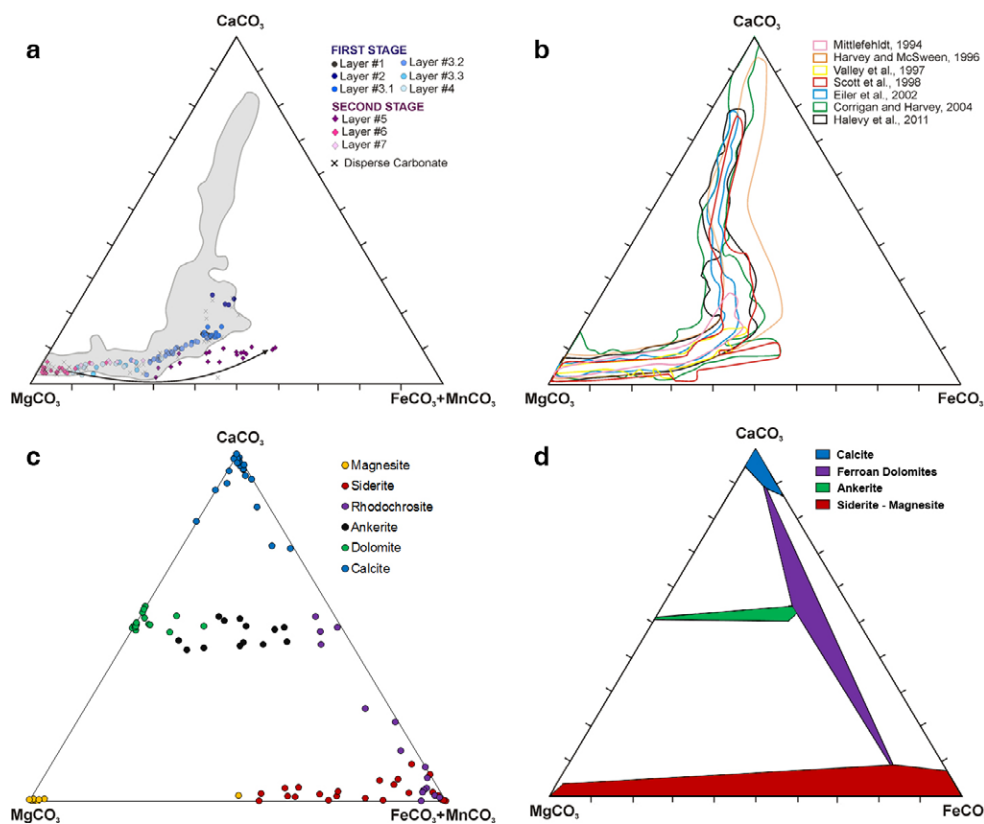


Fig. 10. a) Ternary diagrams showing the data obtained by electron microprobe from around 160 different spots (see J7.1 and D5.ex in Fig. 5 and Table 2). Note the progressive compositional change between layers #1 and #4 and the sharp compositional change between layers #4 and #5 (black arrow). The shaded area shows published carbonate compositions of ALH 84001 (based on data published by Holland et al. [1999, 2005] who plotted Fe+Mn contents). b) Ternary diagram showing, in different colors, carbonate compositions of ALH 84001 published by different authors (Mittlefehldt 1994; Harvey and McSween 1996; Valley et al. 1997; Scott et al. 1998; Eiler et al. 2002; Corrigan and Harvey 2004; Halevy et al. 2011), who only plotted Fe contents. c) Compositions of several terrestrial carbonates (data taken from Chang et al. 1996). d) Distribution of the calcite solid solutions (blue), ferroan dolomites with less than 20% Fe substitution (purple), ankerite solid solutions (green), and siderite-magnesite solid solutions (red), at 450 °C (adapted from Rosenberg 1967). The diagrams show the mole% of  $\text{MgCO}_3$ ,  $\text{CaCO}_3$ ,  $\text{FeCO}_3$ , and  $\text{MnCO}_3$ .

lower, the precipitation of a more Ca- and Mn-rich carbonate started (layer #2). After that, successive layers are progressively depleted in Fe and Mn and enriched in Mg (layers #2 to #4, and posteriorly #5 to #6), representing precipitation from an evolving fluid, which was progressively depleted on Fe and Mn as carbonate precipitated. Thus, the sharp change from Fe- and Mn-poor layer #4 to the Fe- and Mn-rich layer #5, would imply the input of a new fluid. Indeed, the presence of small fractures and local corrosion formed prior to layer #5 (Fig. 6) strongly suggest that a new hydrous event introduced a Fe-rich fluid into the system, responsible for the precipitation of layers #5 and #6. The possibility of an additional fluid influx between layers #6 and #7 (layer #7 has higher Fe and Mn content than layer #6) cannot be discounted. This interpretation is in accordance with experimental data obtained by Golden et al. (2001), who performed a

multiple step precipitation process to produce chemically and mineralogically zoned synthetic carbonate globules (see their table 1; fig. 1). In the first step they added Ca, Fe, and Mg to the starting solution, and as a result a globule with a Ca-Fe-rich core precipitated, progressively grading outwards to a more Mg-rich carbonate.

Small high atomic number inclusions occur between carbonate layers #4 and #5 (Fig. 6, D5.5), but their small size prevented identification. We believe that they could be the pyrrhotite and/or magnetite inclusions that other authors have observed in carbonate rosette rims, which are interpreted to have possibly precipitated when the carbonate was invaded and partially melted by shock-generated liquids (McKay and Lofgren 1997; Scott et al. 1997a; Bradley et al. 1998). Indeed, the small fractures observed in Fig. 6 (red arrows) are consistent with shock between the precipitation of layers



#4 and #5. These apparently amorphous magnetite inclusions, intermixed with iron sulfide, and the voids where they formed, can be the direct result of local carbonate decomposition by an impact (Scott et al. 1997b; Barber and Scott 2002). However, a strong shock melting of the carbonates would make the borders of layer #4 corroded and anhedral, but the boundary between layers #4 and #5 is mostly euhedral. The melting produced by shock should then have been of submicrometer scale.

Microprobe data reveal that the studied carbonates fall between dolomite, ankerite, siderite and magnesite (Figs. 5 and 10; Tables 1 and 2) whereas calcite, the most common terrestrial carbonate, is absent. The compositions of ALH 84001,82 carbonates do not correspond to any known mineral (Harvey and McSween 1996). Also, there is no solid solution series in terrestrial carbonates from calcite to dolomite or ankerite, and nor from those minerals to magnesite or siderite (see e.g., Chang et al. 1996). Therefore, there is no mineral intermediate between these phases, because the substitution of Ca by Mg or Fe is not straightforward. These carbonates with intermediate compositions are unusual on Earth, and their presence suggests a terrestrially uncommon formation scenario. For example, different and variable aqueous solutions under changing environmental circumstances (see e.g., Fernández-Remolar et al. 2011) supported by kinetic stabilization of these metastable compositions (McKay and Lofgren 1997). Compositionally similar carbonate globules have been found on Earth in specific contexts like the volcanic centers in Spitsbergen (Norway), and other few places (Treiman et al. [2002] and references therein). Those carbonates are also described as discs, with cores called “ASM” because of their compositions lying between ankerite, siderite, and magnesite (Treiman et al. 2002).

Our findings suggest that, over time, fluids with different compositions soaked the host rock of this meteorite, possibly indicating distinct aqueous alteration events. This hypothesis should be further explored in light of new data from orbiters and rovers, and laboratory analysis of meteorites.

## CONCLUSIONS

ALH 84001 is the oldest (4.1 Gyr old) known Martian meteorite and so is a unique source of information on the environmental conditions of early Mars. The main conclusions from this study are as follows:

1. The presence of two sets of fractures in this igneous achondrite support previous studies showing that its constituent minerals have suffered at least two shock events.
2. Carbonate globules, located between cracks in the rock, formed by precipitation from a Mg- and Fe-rich aqueous solution. The euhedral shape observed at the boundary between layers #4 and #5, together with the sharp change in composition, implies precipitation during at least two episodes and from different generations of fluids. Small inclusions at the margins of layer #4, described by other authors as magnetite and sulfide, together with small fractures that do not extend from layer #4 to #5, are explained by a shock event that created the fractures and introduced a second fluid, which precipitated further carbonate as layers #5 and #6, at least. Layer #7 could be the result of a third precipitation event from a later fluid, but the evidence is less clear.
3. The evidence compiled here demonstrates a temporally differentiated fluid environment within the region of the Martian crust that was sampled by ALH 84001. Two, or possibly three, generations of fluids formed the carbonates in different stages. Carbonate precipitation incrementally changed the aqueous environment to promote the precipitation of more Fe- and Mg-rich carbonates. Our model is consistent with the previous studies suggesting a hydrothermal origin for the carbonates.
4. ALH 84001 carbonates have been previously related to specific minerals, such as siderite and dolomite. In common with some previous studies, our data suggest the presence of a mineral with composition that is uncommon on Earth. This phase evolves across the immiscibility areas between Fe-, Mg- and Ca-rich carbonates, constituting metastable minerals that require a more comprehensive characterization, opening the door to future analysis on ALH 84001.
5. CL is a very useful technique for locating and characterizing carbonates in ALH 84001, and specific compositional zones within them, and it should be considered for use in studies of other carbonate-bearing Martian meteorites.

*Acknowledgments*—This research has been funded by the Spanish Ministry of Science and Innovation (projects: AYA2011-26,522, AYA 2015-67175-P, CTQ2015-62,635-ERC, and CTQ2014-60,119-P to which J.M. Trigo-Rodríguez and C.E. Moyano-Camero acknowledge financial support). The UK Science and Technology Facilities Council is also thanked for funding through grants ST/H002960/1, ST/K000942/1, and ST/L002167/1. ICN2 and ICMAB acknowledge support of the Spanish MINECO through the Severo Ochoa Centers of Excellence Program under Grants SEV-2013-0295 and SEV-2015-0496, respectively. We acknowledge B. Ballesteros and M.

Rosado from the ICN2 Electron Microscopy Division, and A. Fernández from the ICTS (National Center of Electronic Microscopy) for the SEM, EDS, and microprobe measurements. We also thank the NASA Meteorite Working Group, and the Johnson Space Center for providing the ALH 84001,82 section. This study was done in the frame of a PhD on Physics at the Autonomous University of Barcelona (UAB) under the direction of J. M. Trigo-Rodríguez.

*Editorial Handling*—Dr. Michael Zolensky

## REFERENCES

- Agee C. B., Wilson N. V., McCubbin F. M., Ziegler K., Polyak V. J., Sharp Z. D., Asmerom Y., Nunn M. H., Shaheen R., Thiemens M. H., Steele A., Fogel M. L., Bowden R., Glamoclija M., Zhang Z., and Elardo S. M. 2013. Unique meteorite from early Amazonian Mars: Water-rich basaltic breccia Northwest Africa 7034. *Science* 339:780–785.
- Akridge D. G., Akridge J. M. C., Batchelor J. D., Benoit P. H., Brewer J., DeHart J. M., Keck B. D., Jie L., Meier A., Penrose M., Schneider D. M., Sears D. W. G., Symes S. J. K., and Yanhong Z. 2004. Photomosaics of the cathodoluminescence of 60 sections of meteorites and lunar samples. *Journal of Geophysical Research* 109:7.
- Bandfield J. L., Glotch T. D., and Christensen P. R. 2003. Spectroscopic identification of carbonate minerals in the martian dust. *Science* 301:1084–1087.
- Barber D. J. and Scott E. R. D. 2002. Origin of supposedly biogenic magnetite in the Martian meteorite Allan Hills 84001. *Proceedings of the National Academy of Sciences* 99:6556–6561.
- Berk W., Ilger J.-M., Fu Y., and Hansen C. 2010. Decreasing CO<sub>2</sub> partial pressure triggered Mg-Fe-Ca carbonate formation in ancient Martian crust preserved in the ALH 84001 Meteorite. *Geofluids* 11:6–17.
- Bogard D. D. and Johnson P. 1983. Martian gases in an Antarctic meteorite? *Science* 221:651–654.
- Borg L. E., Connelly J. N., Nyquist L. E., Shih C.-Y., Wiesmann H., and Reese Y. 1999. The age of the carbonates in the Martian meteorite ALH 84001. *Science* 286:90–94.
- Boynton W. V., Ming D. W., Kounaves S. P., Young S. M. M., Arvidson R. E., Hecht M. H., Hoffman J., Niles P. B., Hamara D. K., Quinn R. C., Smith P. H., Sutter B., Catling D. C., and Morris R. V. 2009. Evidence for calcium carbonate at the Mars Phoenix landing site. *Science* 325:61–64.
- Bradley J. P., McSween H. Y. Jr, and Harvey R. P. 1998. Epitaxial growth of nanophase magnetite in Martian meteorite Allan Hills 84001: The implications for biogenic mineralization. *Meteoritics & Planetary Science* 33:765–773.
- Bridges J. C. and Grady M. M. 2000. Evaporite mineral assemblages in the nakhlite (Martian) meteorites. *Earth and Planetary Science Letters* 176:267–279.
- Bridges J. C. and Schwenzer S. P. 2012. The nakhlite hydrothermal brine on Mars. *Earth and Planetary Science Letters* 359–360:117–123.
- Bridges J. C., Catling D. C., Saxton J. M., Swindle T. D., Lyon I. C., and Grady M. M. 2001. Alteration assemblages in Martian meteorites: Implications for near-surface processes. *Space Science Reviews* 96:365–392.
- Brodie K., Fette D., Harte B., and Schmid R. 2007. 3. Structural terms including fault rock terms. Recommendations by the IUGS Subcommittee on the Systematics of Metamorphic Rock, web version: 1–14.
- Burns R. 1969. *Mineralogical applications of crystal field theory*. New York: Cambridge University Press. p. 551.
- Carr R. H., Grady M. M., Wright I. P., and Pillinger C. T. 1985. Martian atmospheric carbon dioxide and weathering products in Mars meteorites. *Nature* 314:248–250.
- Chang L. L. Y., Howie R. A., and Zussman J. 1996. *Non-silicates: Sulphates, carbonates, phosphates and halides*. London: The Geological Society. p. 383.
- Chatzitheodoridis E. and Turner G. 1990. Secondary minerals in the Nakhla meteorite. *Meteoritics* 25:354.
- Cooney T. F., Scott E. R. D., Krot A. N., Sharma S. K., and Yamaguchi A. 1999. Vibrational spectroscopic study of minerals in the Martian meteorite ALH 84001. *American Mineralogist* 84:1569–1576.
- Corrigan C. M. and Harvey R. P. 2004. Multi-generational carbonate assemblages in Martian meteorite Allan Hills 84001: Implications for nucleation, growth and alteration. *Meteoritics & Planetary Science* 39:17–30.
- Corrigan C. M., Niles P. B., Leshin L. A., Harvey R. P., Guan Y., and McKeegan K. D. 2003. Oxygen isotopic compositions of unique carbonates in Martian meteorite Allan Hills 84001 (abstract #5269). *Meteoritics & Planetary Science* 38.
- Downs R. T. 2006. The RRUFF Project: An integrated study of the chemistry, crystallography, Raman and infrared spectroscopy of minerals (abstract). Program and Abstracts of the 19th General Meeting of the International Mineralogical Association. pp. 3–13.
- Ehlmann B. L., Mustard J. F., Murchie S. L., Poulet F., Bishop J. L., Brown A. J., Calvin W. M., Clark R. N., Des Marais D. J., Milliken R. E., Roach L. H., Roush T. L., Swayze G. A., and Wray J. J. 2008. Orbital identification of carbonate-bearing rocks on Mars. *Science* 322:1828–1832.
- Eiler J., Valley J. W., Graham C. M., and Fournelle J. 2002. Two populations of carbonate in ALH 84001: Geochemical evidence for discrimination and genesis. *Geochimica et Cosmochimica Acta* 66:1285–1303.
- Fernández-Remolar D. C., Sánchez-Román M., Hill A. C., Gómez-Ortiz D., Prieto Ballesteros O., Romanek C. S., and Amils R. 2011. The environment of early Mars and the missing carbonates. *Meteoritics & Planetary Science* 46:1447–1469.
- Frey H. V. 2008. Ages of very large impact basins on Mars: Implications for the late heavy bombardment in the inner solar system. *Geophysical Research Letters* 35:L13203.
- Golden D. C., Ming D. W., Schwandt C. S., Morris R. V., Yang S. V., and Lofgren G. E. 2000. An experimental study of kinetically-driven precipitation of calcium-magnesium-iron carbonates from solution: Implications for the low-temperature formation of carbonates in Martian meteorite Allan Hills 84001. *Meteoritics & Planetary Science* 35:457–465.
- Golden D. C., Ming D. W., Schwandt C. S., Lauer H. V., Socki R. A., Morris R. V., Lofgren G. E., and McKay G. A. 2001. A simple inorganic process for the formation of

- carbonates, magnetite, and sulfides in Martian meteorite ALH 84001. *American Mineralogist* 86:370–375.
- Götze J., Krbetscheck M. R., Habermann D., and Wolf D. 2000. High-resolution cathodoluminescence studies of feldspar minerals. In *Cathodoluminescence in geosciences*, edited by Pagel M., Barbin V., Blanc P., and Ohnenstetter D. New York: Springer-Verlag. pp. 245–270.
- Greenwood J. P. and McSween H. Y. 2001. Petrogenesis of Allan Hills 84001: Constraints from impact melted feldspathic and silica glasses. *Meteoritics & Planetary Science* 36:43–61.
- Halevy I., Fischer W. W., and Eiler J. M. 2011. Carbonates in the Martian meteorite Allan Hills 84001 formed at  $18 \pm 4$  °C in a near-surface aqueous environment. *Proceedings of the National Academy of Sciences of the United States of America* 108:16,895–16,899.
- Hall A. 1987. *Igneous petrology*. London: Longman Publishers. pp. 228–231.
- Hamilton V. E., Christensen P. R., McSween H. Y., and Bandfield J. L. 2003. Searching for the source regions of Martian meteorites using MGS TES: Integrating Martian meteorites into the global distribution of igneous materials on Mars. *Meteoritics & Planetary Science* 38:871–885.
- Harvey R. P. and McSween H. Y. 1996. A possible high-temperature origin for the carbonates in the Martian meteorite ALH 84001. *Nature* 382:49–51.
- Holland G., Lyon I. C., Saxton J. M., and Turner G. 1999. Evidence for an unusual generation of carbonate in Allan Hills 84001 (abstract). *Meteoritics & Planetary Science* 34:A55–56.
- Holland G., Saxton J. M., Lyon I. C., and Turner G. 2005.  $\delta^{18}\text{O}$  values in Allan Hills 84001 carbonate: Possible evidence for water precipitation on Mars. *Geochimica et Cosmochimica Acta* 69:1359–1369.
- Jull A. J. T., Eastoe C. J., Xue S., and Herzog G. F. 1995. Isotopic composition of carbonates in the SNC meteorites Allan Hills 84001 and Nakhla. *Meteoritics & Planetary Science* 30:311–318.
- Kring D. A. and Gleason J. D. 1997. Magmatic temperatures and compositions on early Mars as inferred from the orthopyroxene-silica assemblage in Allan Hills 84001 (abstract). *Meteoritics & Planetary Science* 32:A74.
- Laetsch T. A. and Downs R. T. 2006. Software for identification and refinement of cell parameters from powder diffraction data of minerals using the RRUFF Project and American Mineralogist Crystal Structure Databases (abstract). Program and Abstracts of the 19th General Meeting of the International Mineralogical Association. pp. 8–25.
- Lapen T. J., Righter M., Brandon A. D., Debaille V., Beard B. L., Shafer J. T., and Peslier A. H. 2010. A younger age for ALH 84001 and its geochemical link to shergottites sources in Mars. *Science* 328:347–351.
- Lee M. R., Tomkinson T., Mark D. F., Stuart F. M., and Smith C. L. 2013. Evidence for silicate dissolution on Mars from the Nakhla meteorite. *Meteoritics and Planetary Science* 48:224–240.
- Machel H. G., Mason R. A., Mariano A. N., and Mucci A. 1991. Causes and measurements of luminescence in calcite and dolomite. In *Luminescence microscopy and spectroscopy: Qualitative and quantitative applications*, edited by Barker C. E. and Kopp O. C. Tulsa, Oklahoma: SEPM Short Course 25:9–25.
- Martel J., Young D., Peng H. H., Wu C. Y., and Young J. D. 2012. Biomimetic properties of minerals and the search for life in the Martian meteorite ALH 84001. *Annual Review of Earth and Planetary Science Letters* 40:167–193.
- McKay G. A. and Lofgren G. E. 1997. Carbonates in ALH 84001: Evidence for kinetically controlled growth (abstract #1799). *28th Lunar and Planetary Science Conference*. CD-ROM.
- McKay D. S., Gibson E. K. Jr, Thomas-Keptra K. L., Vali H., Romanek C. S., Clemett S. J., Chillier X. D. F., Maechling C. R., and Zare R. N. 1996. Search for past life on Mars: Possible relic biogenic activity in Martian meteorite ALH 84001. *Science* 273:924–930.
- McSween H. Y. 1994. What we have learned about Mars from SNC meteorites. *Meteoritics & Planetary Science* 29:757–779.
- Melosh H. J. 1984. Impact ejection, spallation, and the origin of meteorites. *Icarus* 59:234–260.
- Meyer C. 2012. ALH 84001. In *Martian meteorite compendium*. <https://curator.jsc.nasa.gov/antmet/mmc/>.
- Michalski J. R. and Niles P. B. 2010. Deep crustal carbonate rocks exposed by meteor impact on Mars. *Nature: Geoscience* 3:751–755.
- Mittlefehldt D. W. 1994. ALH 84001, a cumulate orthopyroxenite member of the SNC meteorite group. *Meteoritics & Planetary Science* 28:214–221.
- Mittlefehldt D. W. 1997. Macroscopic description of Allan Hills 84001 and the relative timing of events in its history (abstract). *Meteoritics & Planetary Science* 32:A93.
- Morris R. V., Ruff S. W., Gellert R., Ming D. W., Arvidson R. E., Clark B. C., Golden D. C., Siebach K., Klingelhöfer G., Schröder C., Fleischer I., Yen A. S., and Squyres S. W. 2010. Identification of carbonate-rich outcrops on Mars by the Spirit rover. *Science* 329:421.
- Moyano-Camero C. E., Trigo-Rodríguez J. M., Benito M., Mestres N., Alonso-Azcárate J., Fraxedas J., and Martín-Torres F. J. 2014. Raman spectroscopy study of the carbonate globules in Allan Hills 84001 to better understand their mineralogy (abstract #1844). *45th Lunar and Planetary Science Conference*. CD-ROM.
- Niles P. B., Leshin L. A., and Guan Y. 2005. Microscale carbon isotopic variability in ALH84001 carbonates and a discussion of possible formation environments. *Geochimica et Cosmochimica Acta* 69:2931–2944.
- Niles P. B., Zolotov M. Y., and Leshin L. A. 2006. The role of CO<sub>2</sub> in aqueous alteration of ultra-mafic rocks and the formation of Mg-Fe-rich aqueous solutions on early Mars (abstract #1440). *37th Lunar and Planetary Science Conference*. CD-ROM.
- Niles P. B., Zolotov M. Y., and Leshin L. A. 2009. Insights into the formation of Fe- and Mg-rich aqueous solutions on early Mars provided by the ALH 84001 carbonates. *Earth and Planetary Science Letters* 286:122–130.
- Nyquist L. E., Bogard D. D., Shih C. Y., Greshake A., Stöffler D., and Eugster O. 2001. Ages and geologic histories of Martian meteorites. *Space Science Reviews* 96:105–164.
- Owen T., Biemann K., Rushneck D. R., Biller J. E., Howarth D. W., and Lafleur A. L. 1977. The composition of the atmosphere at the surface of Mars. *Journal of Geophysical Research* 82:6435–6439.
- Rimstidt J. D., Balog A., and Webb J. 1998. Distribution of trace elements between carbonate minerals and aqueous solutions. *Geochimica et Cosmochimica Acta* 62:1851–1863.
- Romanek C. S., Thomas K. L., Gibson E. K., McKay D. S., and Socki R. A. 1995. Petrogenesis of carbon and sulfur-



- bearing minerals in the Martian meteorite ALH 84001 (abstract #1183). 26th Lunar and Planetary Science Conference. CD-ROM.
- Rosenberg P. E. 1967. Subsolidus relations in the system  $\text{CaCO}_3\text{-MgCO}_3\text{-FeCO}_3$  between 350° and 550 °C. *The American Mineralogist* 52:787–796.
- Saxton J. M., Lyon I. C., and Turner G. 1998. Correlated chemical and isotopic zoning in carbonates in the Martian meteorite ALH 84001. *Earth and Planetary Science Letters* 160:811–822.
- Schwandt C. S., McKay G. A., and Lofgren G. E. 1999. FESEM imaging reveals previously unseen detail and enhances interpretations of ALH 84001 carbonate petrogenesis (abstract #1346). 30th Lunar and Planetary Science Conference. CD-ROM.
- Score R. and MacPherson G. 1985. Macroscopic and thin section description of ALH 84001. In *Antarctic meteorite newsletter 8* (vol. 2), edited by Satterwhite C. and Righter K. Houston, Texas: NASA Johnson Space Center. 5p.
- Scott E. R. D., Yamaguchi A., and Krot A. N. 1997a. Petrological evidence for shock melting of carbonates in the Martian meteorite ALH 84001. *Nature* 387:377–379.
- Scott E. R. D., Yamaguchi A., and Krot A. N. 1997b. Shock melting of carbonate, plagioclase and silica in the Martian meteorite ALH 84001 (abstract #1789). 28th Lunar and Planetary Science Conference. CD-ROM.
- Scott E. R. D., Krot A. N., and Yamaguchi A. 1998. Carbonates in fractures of Martian meteorite ALH 84001: Petrologic evidence for impact origin. *Meteoritics & Planetary Science* 33:709–719.
- Steele A., Fries M. D., Amundsen H. E. F., Mysen O., Fogel M. L., Schweizer M., and Boctor N. Z. 2007. Comprehensive imaging and Raman spectroscopy of carbonate globules from Martian meteorite ALH 84001 and a terrestrial analogue from Svalbard. *Meteoritics & Planetary Science* 42:1549–1566.
- Theis K. J., Lyon I., Burgess R., and Turner G. 2008. Iron isotopic fractionation of zoned carbonates from ALH 84001 (abstract). *Meteoritics & Planetary Science* 43:A153.
- Tomkinson T., Lee M. R., Mark D. F., and Smith C. L. 2013. Sequestration of Martian  $\text{CO}_2$  by mineral carbonation. *Nature Communications* 4:2662.
- Treiman A. H. 1995. A petrographic history of Martian meteorite ALH 84001: Two shocks and an ancient age. *Meteoritics & Planetary Science* 30:294–302.
- Treiman A. H. 1998. The history of Allan Hills 84001 revised: Multiple shock events. *Meteoritics & Planetary Science* 33:753–764.
- Treiman A. H., Gleason J. D., and Bogard D. D. 2000. The SNC meteorites are from Mars. *Planetary and Space Science* 48:1213–1230.
- Treiman A. H., Amundsen H. E. F., Blake D. F., and Bunch T. 2002. Hydrothermal origin for carbonate globules in Martian meteorite ALH 84001: A terrestrial analogue from Spitsbergen (Norway). *Earth and Planetary Science Letters* 204:323–332.
- Valley J. W., Eiler J. M., Graham C. M., Gibson E. K., Romanek C. S., and Stolper E. M. 1997. Low-temperature carbonate concretions in the Martian meteorite ALH 84001: Evidence from stable isotopes and mineralogy. *Science* 275:1633–1637.
- Warren P. H. 1998. Petrologic evidence for low-temperature, possibly flood evaporitic origin of carbonates in the ALH 84001 meteorite. *Journal of Geophysical Research* 103:16,759–16,773.
- Weiss B. P., Vali H., Baudenbacher F. J., Kirschvink J. L., Stewart S. T., and Schuster D. L. 2002. Records of an ancient Martian magnetic field in ALH 84001. *Earth and Planetary Science Letters* 201:449–463.
- Wray J. J., Murchie S. L., Ehlmann B. L., Milliken R. E., Seelos K. D., Dobrea E. Z. N., Mustard J. F., and Squyres S. W. 2011. Evidence for regional deeply buried carbonate-bearing rocks on Mars (abstract #2635). 42nd Lunar and Planetary Science Conference. CD-ROM.

## SUPPORTING INFORMATION

Additional supporting information may be found in the online version of this article:

**Fig S1:** High-resolution CL mosaic of the ALH 84001,82 thin section that can be compared directly with Fig. 1. Bright red areas correspond to very Fe-

poor and Mn-rich layers in carbonates.

**Table S1:** Position (in  $\text{cm}^{-1}$ ) of the main peaks found by Raman spectroscopy (see Fig. 4). Those in bold were clearly distinguishable from noise before the background was removed. Other minor peaks, plus some whose origin has not been determined, are not listed.